NeuroImage: Clinical 8 (2015) 560–571

Contents lists available at ScienceDirect

NeuroImage: Clinical

journal homepage: www.elsevier.com/locate/ynicl

Network analysis of EEG related functional MRI changes due to medication withdrawal in focal epilepsy

Kees Hermans[a,b,*], Pauly Ossenblok[c], Petra van Houdt[a,b], Liesbeth Geerts[d], Rudolf Verdaasdonk[b], Paul Boon[a], Albert Colon[e], Jan C. de Munck[b]

[a] Department of Research and Development, Academic Center for Epileptology, Kempenhaeghe & Maastricht UMC+, Heeze, The Netherlands
[b] Department of Physics and Medical Technology, VU University Medical Center, Amsterdam, The Netherlands
[c] Department of Clinical Physics, Academic Center for Epileptology, Kempenhaeghe & Maastricht UMC+, Heeze, The Netherlands
[d] MR Neuro Imaging, Philips Healthcare, Best, The Netherlands
[e] Department of Neurology, Academic Center for Epileptology, Kempenhaeghe & Maastricht UMC+, Heeze, The Netherlands

ARTICLE INFO

Article history:
Received 12 December 2014
Received in revised form 5 May 2015
Accepted 2 June 2015
Available online 9 June 2015

Keywords:
Epilepsy
EEG–fMRI
Anti-epileptic drugs
Functional connectivity
Resting-state fMRI

ABSTRACT

Anti-epileptic drugs (AEDs) have a global effect on the neurophysiology of the brain which is most likely reflected in functional brain activity recorded with EEG and fMRI. These effects may cause substantial inter-subject variability in studies where EEG correlated functional MRI (EEG–fMRI) is used to determine the epileptogenic zone in patients who are candidate for epilepsy surgery. In the present study the effects on resting state fMRI are quantified in conditions with AED administration and after withdrawal of AEDs.

EEG–fMRI data were obtained from 10 patients in the condition that the patient was on the steady-state maintenance doses of AEDs as prescribed (condition A) and after withdrawal of AEDs (condition B), at the end of a clinically standard pre-surgical long term video-EEG monitoring session. Resting state networks (RSN) were extracted from fMRI. The epileptic component (ICE) was identified by selecting the RSN component with the largest overlap with the EEG–fMRI correlation pattern. Changes in RSN functional connectivity between conditions A and B were quantified.

EEG–fMRI correlation analysis was successful in 30% and 100% of the cases in conditions A and B, respectively. Spatial patterns of ICEs are comparable in conditions A and B, except for one patient for whom it was not possible to identify the ICE in condition A. However, the resting state functional connectivity is significantly increased in the condition after withdrawal of AEDs (condition B), which makes resting state fMRI potentially a new tool to study AED effects. The difference in sensitivity of EEG–fMRI in conditions A and B, which is not related to the number of epileptic EEG events occurring during scanning, could be related to the increased functional connectivity in condition B.

1. Introduction

If the epilepsy of drug resistant patients is focal a possible therapy is the surgical resection of the epileptogenic zone. A promising new tool to detect the epileptogenic zone is the recording of simultaneous EEG and functional MRI (EEG–fMRI) (Rosenkranz and Lemieux, 2010; Salek-Haddadi et al., 2003; Zijlmans et al., 2007) in which the high spatial resolution of fMRI is directly coupled to the high temporal resolution of EEG. This is achieved by correlating the occurrence of interictal epileptic discharges (IED) in the EEG to the fMRI signals using a general linear model (GLM) framework.

Validation studies have been performed with EEG–fMRI using both implanted depth electrodes (SEEG) (van Houdt et al., 2012) and electrocorticography (ECoG) (Bénar et al., 2006; van Houdt et al., 2013) as gold standard. Although generally good agreement has been found, there is also substantial variability in the EEG–fMRI yield, which may be related to the varying number of IEDs (van Houdt et al., 2010). Furthermore, the shape and sign of the hemodynamic response function (HRF) may vary from patient to patient (Aguirre et al., 1998; Bagshaw et al., 2004). A possible reason for the generally observed large variability in between patients might be that the patient group of drug resistant epilepsy patients is an inhomogeneous group characterized by differences in semiology, and kinds and doses of anti-epileptic drugs (AEDs).

To our knowledge no studies have been reported on effects of AEDs on resting state fMRI, whereas the effect of other types of medication on the central nervous system has been studied by analyzing the fMRI signals of healthy subjects in a resting state. Khalili-Mahani et al. (2012),

* Corresponding author at: Department of Research and Development, Kempenhaeghe, Postbus 61, 5590 AB Heeze, The Netherlands. Tel.: +3 140 227 9548.
E-mail address: HermansKe@kempenhaeghe.nl (K. Hermans).

http://dx.doi.org/10.1016/j.nicl.2015.06.002

for example, used functional connectivity analysis based on the time series of ICs to investigate the effect of drugs and alcohol in healthy volunteers and found significant changes in rsFC after intake of morphine and alcohol, whereas Cole et al. (2013) showed that differences in dopamine concentrations in the (healthy) human brain can be detected based on functional connectivity of resting state networks (RSNs). Finally, Mueller et al. (2014) reported the effects of methylphenidate on RSN functional connectivity, using the same approach. Our goal was to conduct a feasibility study and to demonstrate the potential of resting state fMRI measures in studying the effect of AEDs.

The standard clinical procedure for presurgical candidates is to apply EEG video monitoring to detect the seizure onset zone. In order to increase the number of seizures AEDs are withdrawn for these patients during the seizure monitoring session. This provided the opportunity to study the effects of AEDs on EEG and fMRI, because the EEG–fMRI recordings can be planned in this period without extra ethical objections. It has been reported that the number of IEDs increases after the occurrence of seizures (Jacobs et al., 2012; Zijlmans et al., 2007). Some research groups plan on purpose the EEG–fMRI during the EEG-video monitoring session, because they presume an increased sensitivity, caused by a presumed increased number of IEDs during the scanning session (e.g. Hunyadi et al., 2013). However, no systematic comparison has been made so far between the condition with and without the administration of AEDs. We investigated the spatiotemporal changes in resting state fMRI due to withdrawal of AEDs using the combined EEG–fMRI data recorded in a condition with medication and at the end of a standard video-EEG seizure monitoring session after medication withdrawal.

We are primarily interested in a comparison of significantly correlated EEG–fMRI patterns. However, such an approach would require successful EEG–fMRI data in both conditions, for all patients. This is difficult to achieve because sufficient IEDs are not always available or the EEG may be unusable because it is contaminated with too much noise due to motion artifacts. We therefore chose a study design where EEG–fMRI was successful in at least one condition, and applied a recently developed data driven approach, spatial ICA of resting state fMRI, to detect the epileptic independent component (ICE) representing the epileptogenic zone (Huishi Zhang et al., 2014; Hunyadi et al., 2013; LeVan and Gotman, 2009; Rodionov et al., 2007; van Houdt et al., 2014). This design enabled us to compare the spatial distributions of the ICE obtained in the conditions with the use of AEDs (condition A) and after withdrawal of AEDs (condition B). Moreover, this approach makes it possible, analogous to previous fMRI drug studies (Cole et al., 2010), to quantify changes in functional connectivity between all components of the resting state networks (RSN) detected with spatial ICA, including the non-epilepsy related ones, to study the effect of AEDs.

Contrary to standard resting fMRI paradigms which last 5–10 min, the scan duration of EEG–fMRI protocols are usually much longer, typically between 30 and 60 min, to maximize the chances of catching sufficient numbers of IEDs. In the present study we exploit this longer scan duration to allow quantification of differences in the spatiotemporal characteristics at the level of the individual patient in the condition with the use of AEDs and after withdrawal of AEDs, thereby avoiding the ambiguous interpretation of group level differences in an inhomogeneous patient group of drug resistant surgical candidates.

2. Materials and methods

2.1. Subjects

EEG–fMRI data have been acquired for patients with focal epilepsy who were candidates for epilepsy surgery and underwent a presurgical video-EEG examination in Kempenhaeghe (Heeze, The Netherlands). The inclusion criteria for this study were: (1) a sufficient number of IEDs in previous EEG recordings (more than 15/h and less than 300/h); (2) localization-related epilepsy determined from previous EEG recordings; and (3) no suspicion of psychogenic non-epileptic seizures or other neurological disorders. Furthermore, patients with a severe risk of tonic–clonic seizures were excluded from the study. The EEG–fMRI study was approved by the Medical Ethics Committee of the University Medical Centre Utrecht and the local committee of Kempenhaeghe. All patients gave informed consent for the study. Patients were notified that the EEG–fMRI study was not part of the standard pre-surgical evaluation and that it did not influence any of the clinical decisions, such as the surgical resection. EEG–fMRI analysis was decided to be successful if the GLM analysis yielded a statistically significant activation pattern, which consisted of multiple voxels inside the brain. The clinical characteristics of the patients included ($n = 10$: 7 male, ages 39.6 ± 11.9 years) are summarized in Table 1. In Table 1 (column 3) the structural 3 T MRI anatomical abnormalities are presented and the electroclinical hypothesis based on previous EEG-recordings outside the MR scanner (including long term video-EEG monitoring) is presented in column 4.

For comparison, resting state fMRI data were acquired in ten healthy volunteers (4 male, 6 female, age range 19–66 years). This measurement protocol was approved by the Medical Ethics Committee of Maastricht University Medical Center. All volunteers gave informed consent for the study.

2.2. EEG and fMRI acquisition

The EEG–fMRI measurements when the patient was using the AEDs as prescribed were performed either before the start of the video-EEG session, or after completing the video-EEG session, when the patients were taking their usual medication (condition A). The EEG–fMRI session after withdrawal of AEDs (condition B) was always performed immediately after completing the video-EEG session, after the complete withdrawal of AEDs (condition B) and for most patients before the reintroduction of their medication, except for two of the patients (patient 3 and 9) for whom one of their usual AEDs was reintroduced after completing their video-EEG session. The number of days between the EEG–fMRI registrations in conditions A and B (a negative number means registration A was performed after registration B) are indicated in column 5 of Table 1. To be able to assess the brain state of the patients during the EEG–fMRI sessions: 1) we asked patients to stay awake during the 45 min of scanning, 2) the patients were monitored continuously during scanning, and afterwards, and 3) they were asked to fill in a questionnaire with one of the questions being whether they had slept during scanning. For each patient two EEG–fMRI datasets (in conditions A and B) as well as an anatomical T1-weighted MRI were acquired at a 3 T MR scanner (Achieva, Philips Medical Systems, Best). The resting-state fMRI data were acquired for 20–45 min using a T_2*-weighted EPI sequence (TR = 2.5 s; TE = 35 ms; voxel size $3.2 \times 3.2 \times 3$ mm^3; 29–33 adjacent slices; bottom-to-top). The patients were instructed to lay still inside the scanner with their eyes closed during this scan. The T1-weighted MRI was acquired using a spin-echo sequence (reconstructed voxel size $1 \times 1 \times 1$ mm^3, multi slice acquisition of 170 slices, TR 8.4 ms, TE 3.9 ms, flip angle 90°). EEG data were acquired simultaneously with an MRI compatible EEG amplifier (MicroMed, Treviso, Italy) and an EEG cap containing 61 Ag/AgCl electrodes positioned according to an extended 10/20 system. Additionally, three current loops were attached to the cap to measure subtle movements inside the scanner (Masterton et al., 2007). Respiratory signals were obtained using a belt measuring abdominal expansion and vector cardiographic (VCG) signals were recorded using MRI compatible sensors connected to the MR scanner. The VCG signal and the respiratory signal were both sampled with a sample frequency of 500 Hz.

Because rsFC results may be influenced by brain state, we used the EEG to explore to what extent differences in drowsiness and sleep stages could affect our results. In order to enable an EEG expert to determine the wakefulness and sleep stage levels a reduced montage was used. The EEG was subdivided in epochs of 30 s for scoring, band pass filtering between 0.3 and 35 Hz based on the AASM criteria (AASM,

Table 1
Summary of patient clinical data.

Patient	Age/gender	MRI abnormalities	Electroclinical hypothesis	# of days between registrations A and B (B − A)	# of EE_A	Medication A	# of EE_B	Medication B	# of seizures B
1	60/male	–	T-R	9	0	VPA (1800 mg) OCB (1800 mg) CLB (5 mg)	37	–	2
2	46/male	Polymicrogyri F-L, P-L, T-L	T-L, O-L, P-L, F-L	−25	1	PHT (300 mg) LTG (800 mg) OCB (1800 g)	45	–	1
3	49/male	–	T-L	−42	4	LTG (300 mg) LEV (1500 g) OCB (1200 mg)	9	LTG (200 mg)	1
4	43/female	HS-R, 2 drains R	T-R	−20	4	CLB (10 mg) LTG (300 mg) LEV (2000 mg)	5		1
5	22/female	MTS-L	T-L	−2	38	OCB (600 mg)	16		12
6	35/male	–	T-P-O	−23	6	LTG (600 mg) LEV (750 mg) VPA (1500 mg)	20		3
7	38/male	–	Multifocal	−28	7	CLB (10 mg) OCB (2100 mg)	11	–	0
8	30/female	FCD-L	O-R	−84	5	CBZ (400 mg)	14	–	0
9	51/male	CD T-L m	T-L	11	11	PHT (425 mg) OCB (2400 mg)	4	PHT (425 mg)	0
10	22/male	–	Uncertain	−12	14	CLB (10 mg) LTG (550 mg) PGB (150 mg) ZSM (200 mg)	4	–	0

Summary of patient clinical data: age, gender, MRI abnormalities, electroclinical hypothesis based on previous EEG-recordings outside the MR scanner (including long term video-EEG monitoring), number of days (a multiple of 24 h) between the EEG–fMRI registrations in conditions A and B (a negative number means registration A was performed after registration B), number of epileptic events in the EEG in condition A, medication used in condition A, number of epileptic events in the EEG in condition B, medication used in condition B and the number of seizure in the 24 h before the EEG–fMRI in condition B. Abbreviations: MTS = multiple temporal sclerosis; HS = hippocampal sclerosis; FCD = focal cortical dysplasia; CD = cortical dysplasia; R = right; L = left; T = temporal; F = frontal; O = occipital; P = parietal; m = mesial; Ins = insular; VPA = valproate, OCB = oxcarbazepine, CLB = clobazam, PHT = phenytoin, LTG = lamotrigine, LEV = levetiracetam, CBZ = carbamazepine, PGB = pregabaline, ZSM = zonisamide.

2007) and bipolar montages Fp1-TP8 and F8-TP7 leads were used for estimating eye movements (blinks, slow wave eye movements). The alpha, sigma and vertex waves in the EEG were estimated using bipolar F4-TP7, C4-TP7 and O2-TP7 leads. Subtle movements were estimated based on the current loop signals that we also use in this study for subtle movement detection of the patient.

For the healthy volunteers a T1-weighted MRI and resting-state fMRI data were acquired with the same settings, except that the resting-state fMRI session lasted 10 min.

2.3. EEG-correlated fMRI analysis

An overview of the entire analysis pipeline for this study is shown in Fig. 1. EEG and fMRI data were analyzed using a GLM to obtain EEG–fMRI correlation patterns (van Houdt et al., 2012). The preprocessing of EEG and fMRI is indicated in columns 1 and 3, with the subsequent GLM analysis that results in an EEG–fMRI correlation pattern (column 2) using Brain Imaging Analysis Package (http://demunck.info/software/). The gradient and ballistocardiographic artifacts were removed from the raw EEG data with average template subtraction and hierarchical clustering as described in de Munck et al. (2013). Current loop signals were used during visual review to avoid identification of motion artifacts as epileptic events (Masterton et al., 2007). After that, IEDs (spikes, sharp waves, or spike-and-wave discharges) were visually identified in the EEG by an experienced EEG specialist (AC), which resulted in an IED density function (# IEDs per volume scan). If the GLM analysis based on this IED density function was inconclusive the IEDs were clustered into different groups based on their spatial distribution (Van 't Ent et al., 2003). The reference function created for IEDs with similar spatial distributions was correlated to the preprocessed fMRI data through a general linear model framework. In Table 1, columns 6 and 8, the number of IEDs used for the general linear model approach (GLM) analysis are listed. For patient 8 interictal epileptic paroxysms were identified to create the IED density function, which is in accordance to his standard EEG examinations.

The fMRI data were spatially realigned to the first image, then the data were matched to an anatomical scan and spatially smoothed (Gaussian kernel with standard deviation 5 mm). Data points with abrupt head movement (more than 0.5 mm or 0.5 degree change in realignment parameter values) were marked as bad and ignored in the GLM analysis. A finite impulse response (FIR) model was used for modeling the correlation between the fMRI time series resulting from the IED density function (de Munck et al., 2007; van Houdt et al., 2010). For that purpose shifted versions of the IED density function

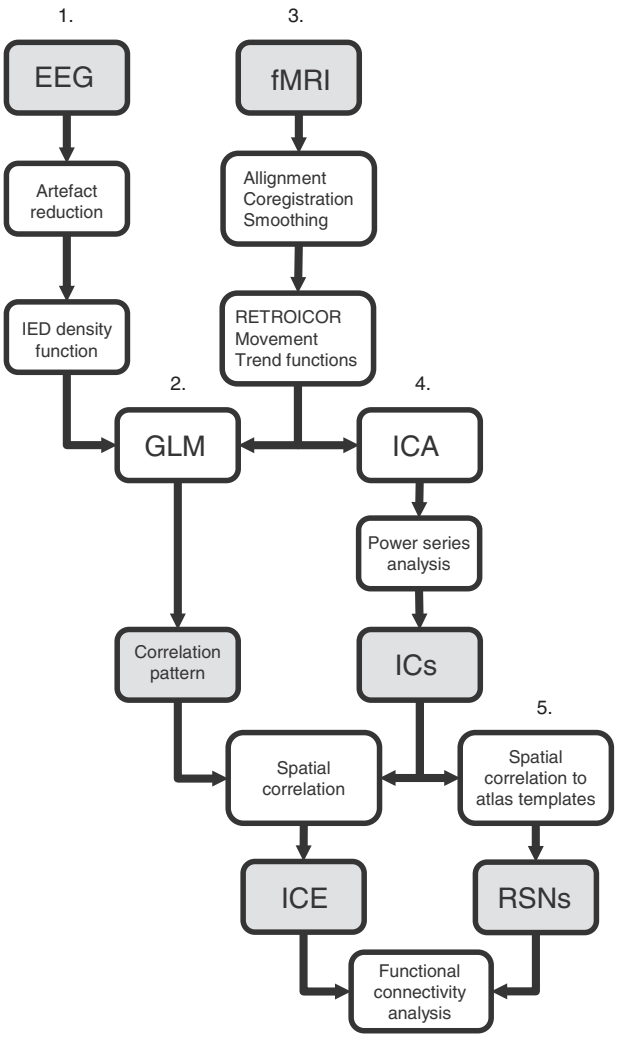

Fig. 1. Schematic overview of analysis pipeline used in this study. GLM = general linear model, ICA = independent component analysis, ICE = epileptic independent component, RSN = resting state network. RETROICOR, movement and trend function time series were regressed out of the data before ICA and GLM analysis.

are included as predictors to the model. To account for the noncausal hemodynamic responses the shifted versions start at −2 time TR (5 s before the IEDs was present in the EEG) and run to +7 times TR (17.5 s after occurrence of the IED in the EEG). The estimated coefficient values of these shifted predictors together represent the maximum likelihood estimate of the HRF.

A constant, linear and quadratic trend, six RETROICOR regressors of heart beat (Glover et al., 2000), ten shifted versions of the heart beat intervals (de Munck et al., 2008) and seven motion regressors resulting from realignment (3 translational, 3 rotational and 1 RMS) were added to the GLM as confounders (Lund et al., 2006). Statistical significance of the parameters of interest was tested using an *F*-test. The false discovery rate (FDR) (Genovese et al., 2002) was calculated based on the *p*-values for the parameters of interest. This FDR was used to threshold the statistical maps (FDR < 0.05).

2.4. Spatial ICA

Spatial ICA was applied to fMRI data to find the ICE and RSNs, as indicated in Fig. 1, column 4. Smoothing and motion correction was performed with SPM5 (Wellcome Department of Imaging Neurosciences, University College London, http://www.fil.ion.ucl.ac.uk/spm). Brain extraction was then performed in FSL (http://www.fmrib.ox.ac.uk/fsl/) to exclude voxels outside the brain from the analysis. Confounding effects were removed from the fMRI time series using a regression analysis (Beall and Lowe, 2010) as implemented in the FEAT toolbox of FSL. The same confounders were used as in the EEG–fMRI analysis (trend functions, RETROICOR, heart beat intervals and motion regressors). The MELODIC toolbox of FSL (Beckmann and Smith, 2004) was used to perform spatial ICA. As a result thresholded *Z*-score component maps, component time series and component power spectra were obtained. The number of ICs of the entire dataset was fixed to 80 components. ICA was performed for the entire 45 min fMRI dataset of the patients, as well as for a selection of 10 min of these data containing the maximum number of IEDs (van Houdt et al., 2014), and for the resting state fMRI of the healthy controls. For the 10 datasets containing a maximum number of IEDs and for the controls the optimal number of ICs was estimated by principal component analysis.

Noise ICs were removed based on the results of power spectrum analysis by comparing the power in a band of interest (Ω_{target} = 0.01–0.08 Hz; Biswal et al., 1995) to the entire power spectrum (Rummel et al., 2013; Tohka et al., 2008):

$$f = \frac{\sum_{\omega_j \in \Omega_{target}} p[\omega_j]}{\sum_{\omega_j \in \Omega} p[\omega_j]}. \quad (1)$$

Here $p[\omega_j]$ is the power at frequency ω_j. ICs with a value of $f < 0.5$ were removed from the analysis.

2.5. Selection of epileptic components and resting state networks

For the detection of the epileptic independent component (ICE) amongst all non-noise components determined by ICA the EEG–fMRI correlation map was used. The spatial correlation $R_k^{EEGfMRI}$ of the EEG–fMRI correlation pattern (A) and all the ICs (IC_k) was calculated, as well as the spatial overlap of the ICE in condition A and B (see Fig. 1, column 3):

$$R_k^{EEGfMRI} = \frac{A \cdot IC_k}{|A||IC_k|} \quad (2)$$

Contrary to van Houdt et al. (2014), who determined the ICE on a combination of resection area and regions of high EEG–fMRI correlation, we used EEG–fMRI overlap alone, because the resection area was not known for all patients. In case of ambiguity, the clinical hypothesis based on previous (video-)EEG recordings was used (Table 1, column 4) to verify the selection of a component. If the EEG–fMRI result showed multiple comparable correlation values with ICs, visual review was used to determine the ICE, based on this clinical hypothesis.

ICs representing RSNs were detected in a similar manner, using the templates from FIND laboratory (Shirer et al., 2012). This set consists of the following RSNs: anterior salience network (aSN), posterior salience network (pSN), auditory network (AN), basal ganglia network (BGN), dorsal default mode network (dDMN), ventral default mode network (vDMN), precuneus network (PrecN), primary visual network (pVN), higher visual network (hVN), visuospatial network (VSN), language network (LN), left executive control network (LECN), right executive control network (RECN), and sensorimotor network (SMN). In order to be able to use these generic templates the spatial maps of the ICs were first normalized to MNI space using SPM5. Spatial correlation of these templates with all the ICs enabled identification of the RSNs (see Fig. 1, column 5). The IC showing the highest correlation value with an RSN template was selected as RSN component for functional connectivity analysis. If all correlation values between an RSN template and the ICs were below 0.25 no RSN component was selected for that particular RSN template. If multiple components showed a correlation value higher than 0.25 only the IC showing the highest value was selected. An example of the result of this RSN selection procedure is shown in Fig. 2. The correlation values of all ICs with the spatial resting state network templates are shown. The columns with correlation values of some ICs have been removed based on the results of the power spectrum analysis procedure which has been explained in Section 2.4.

2.6. Functional connectivity analysis

To determine whether functional connectivity between the RSNs has changed significantly between conditions A and B, we quantified differences in functional connectivity using a GLM approach. In this GLM the linear relationship between two RSN component time series is expressed by a parameter α and the GLM is used to assess whether the same slope parameter in both conditions is adequate, or whether a parameter $\Delta\alpha = \alpha_A - \alpha_B$ is statically significant. In the latter case we conclude that a significant change in functional connectivity has occurred. Details of the GLM can be found in Appendix 1.

2.7. Group analysis

Because ICA will generally result in different RSN components for each subject, a group analysis can only be based on the mean of the network parameters extracted for each subject. We therefore quantified whole brain functional connectivity by averaging the difference parameter $\Delta\alpha$ over all combinations of RSN components for which $\Delta\alpha$ is significant, giving a mean value for the difference parameter $\Delta\alpha$ per subject ($\overline{\Delta\alpha}$). In a formula, we have

$$\overline{\Delta\alpha} = \frac{1}{L}\sum_{i,j\in\Gamma} \Delta\alpha_{i,j} \quad (3)$$

The summation is over the L matrix entries in the subset Γ for which $\Delta\alpha_{i,j}$ is significant. The mean difference parameter $\overline{\Delta\alpha}$ has been calculated for all patients, both for the entire datasets, as well as for the 10 min data selections.

3. Results

3.1. EEG–fMRI results

Of the patients who agreed to participate in the study only those patients are included for whom EEG–fMRI was successful in at least one of the conditions ($n = 10$). In condition A, after the reintroduction of the AED administration, statistical significant EEG–fMRI correlation patterns were obtained for 3 out of the 10 patients. For the remaining 7

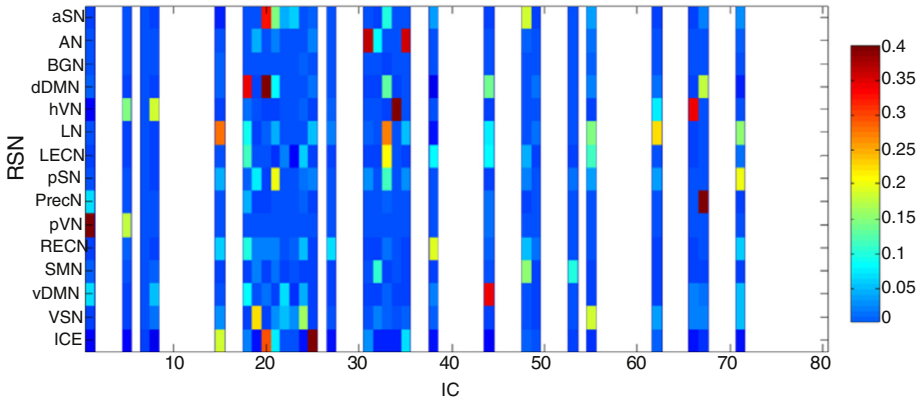

Fig. 2. Example of correlation of RSN templates and the EEG–fMRI result (vertical axis) with the ICs (horizontal axis) found in one patient. Noise components have been removed (white spaces) based on power spectrum (signal power at frequency of interest compared to total power).

patients no statistical significant correlation patterns were found. On the other hand, significant EEG–fMRI correlation results were obtained for all 10 patients for condition B. In condition A on average 9 ± 10 IEDs were detected, and in condition B 17 ± 13 IEDs (Table 1, columns 6 and 8). The number of IEDs was higher in condition B compared to A, but not significantly (Wilcoxon rank sum test gives $p = 0.13$). Listed in Table 1 is also the number of seizures that occurred during the last 24 h before the EEG–fMRI after withdrawal of AEDs (column 10). No seizures occurred in the 24 h before EEG–fMRI in the condition without withdrawal of AEDs, for none of the patients studied.

The EEG–fMRI correlation patterns (of condition B) are shown in column 1 of Fig. 3 and summarized in column 2 of Table 2. For patient 5 the EEG–fMRI correlation pattern of condition A has been used for further analysis. For this patient the GLM analysis of the EEG–fMRI data in condition B was hampered by the huge amount of epileptic discharges occurring in the EEG during scanning, most likely because 12 seizures occurred in the 24 h before the start of EEG–fMRI after medication withdrawal. In general, the spatial pattern of EEG–fMRI, as listed in Table 2 (column 2) is in line with the clinical hypothesis, as listed in column 4 of Table 1. For patients 2, 3, 7, 8 and 9 multiple regions of significant activation were found including more regions than the epileptic onset zone. For patient 2 activation areas are present in the frontal, insular and parietal regions. For patient 3 activation areas in the temporal and parietal region are found. For patients 7 and 9, the largest activation area was present in the left temporal lobe, however also activation areas were present in the right temporal lobe (according to the clinical

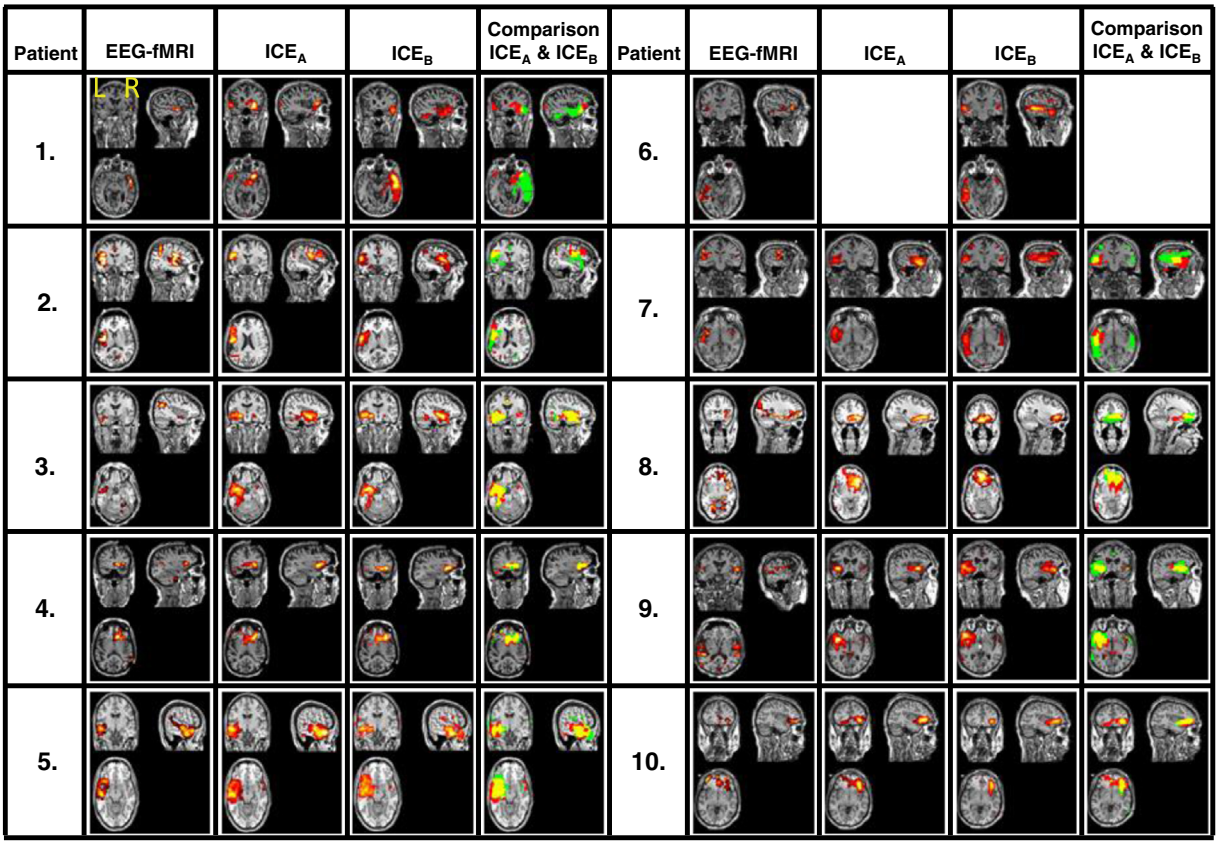

Fig. 3. Spatial patterns of the GLM result, the ICE_A, the ICE_B, and a comparison of ICE_A and ICE_B. In this picture the ICE_A is indicated in red, the ICE_B in green, and their spatial overlap is indicated in yellow. The ICEs are the result of ICA of the entire 45 min datasets.

Table 2
Summary of EEG–fMRI and ICA findings (entire datasets).

Patient	EEG–fMRI	ICE_A	ICE_B	R ICE_A and EEG–fMRI	R ICE_B and EEG–fMRI	R ICE_A and ICE_B
1	T-R	T-R	T-R	0.14	0.31	0.21
2	F-L, Ins-L, P-L	F-L, Ins-L	F-L, Ins-L	0.31	0.37	0.36
3	T-L, P-L	T-L	T-L	0.06	0.07	0.91
4	F-R	F-R	F-R	0.14	0.33	0.82
5	T-L	T-L	T-L	0.76	0.59	0.73
6	T-L	–	T-L, O-L	–	0.1	–
7	T-L, T-R	T-L	T-L, T-R	0.17	0.21	0.17
8	T-R, F-R, P	F-R	F-R	0.15	0.07	0.46
9	T-L, T-R, Ins-L	T-L, Ins-L	T-L, Ins-L	0.05	0.05	0.53
10	F-R, F-L	F-R	F-R	0.20	0.06	0.74

R = right; L = left; T = temporal; F = frontal; O = occipital; P = parietal; m = mesial; Ins = insular.

hypothesis patient 7 has multiple foci). For patient 8 activation areas were found in the frontal and parietal regions, however according to the clinical hypothesis the seizure onset zone is in the occipital region. For patient 10 the electro-clinical hypothesis is uncertain, the EEG–fMRI correlation pattern indicates activation in the frontal region.

3.2. Epileptic independent components

The selected ICEs are presented in Fig. 3, for condition A (ICE_A) in column 2 and condition B (ICE_B) in column 3. The mean spatial correlation of the ICEs with the EEG–fMRI correlation patterns is 0.22 ± 0.20 for condition A and 0.22 ± 0.18 for condition B (columns 4 and 5 of Table 2). A relatively large (>0.2, correlation with other components is typically <0.05) spatial correlation was found between the EEG–fMRI correlation pattern and the ICEs of patients 1, 2, 4, 5 and 7. For patient 3 the spatial correlation is low because a part of the right executive central network coincides with the EEG–fMRI result. For this patient the ICEs of A and B were selected based on the overlap of these components with part of the EEG–fMRI correlation pattern that was located in the left temporal lobe. For patient 6 no ICE could be detected for the fMRI obtained in condition B, probably due to movement during scanning resulting in noisy independent components. The EEG–fMRI correlation pattern of patient 8 contains part of the default mode network, which results in low correlation values with the selected ICs. Therefore, for this patient the frontal part of the EEG–fMRI correlation pattern was used for selection of the ICE. The EEG–fMRI result shows significant activation in the left and right temporal lobe. For this patient an ICE in the left temporal lobe has been selected, which is in accordance with the clinical hypothesis of this patient.

Contrary to EEG–fMRI, the spatial extent of the ICE of all patients is limited to a single region, which appears to coincide, in all cases except for patients 4 and 8, with the clinical hypothesis regarding the onset zone of the epilepsy. For patient 4 the clinical hypothesis was ambiguous and the onset zone could either be located in the temporal lobe, or frontal lobe, or in both. For patient 8 the clinical hypothesis for the location of the focus is in the occipital area, however the EEG–fMRI shows no activation in the occipital area, and the location of the EEG–fMRI result has been chosen for identification of the ICEs. The selected ICEs show a qualitatively clear overlap for conditions A and B (column 4 of Fig. 3). In column 6 of Table 2 the spatial resemblance is quantified between ICE_A and ICE_B The mean correlation of ICE_A with ICE_B is 0.55 ± 0.25, whereas the overlap of the noise components is of the order of 0.05. This indicates that the spatial extent of the ICE in conditions A and B is not substantially affected by drugs withdrawal. In patient 1 the spatial pattern of ICE_A is smaller than the pattern of ICE_B, as is shown in Fig. 3. In patient 7 the spatial pattern of ICE_A lies entirely in the left temporal lobe. The GLM result and the spatial pattern of ICE_B are also partly located in the parietal lobe. It is possible that in patients 1 and 7 the ICEs of condition B incorporates some part of the propagation zone and that the ICE_A only indicates the onset zone. A spatial correlation value could not be calculated for patient 6, because ICEs could not be identified in both conditions for this patient. For patients 1, 2 and 7 the spatial correlation of ICE_A and ICE_B is relatively low as compared to patients 3, 4, 5, 8 and 9. The overlap of the ICEs obtained for conditions A and B is higher than their overlap with the EEG–fMRI correlation pattern, probably because EEG–fMRI may reflect the onset and propagation areas involved in the IEDs, whereas the ICE seems to represent the onset zone of the IEDs.

3.3. Functional connectivity analysis

Functional connectivity analysis was done for nine patients (the result of patient 6 was omitted because no ICE could be detected). An example of functional connectivity analysis results for patient 4 is shown in Fig. 4a, for the 45 min fMRI dataset. For this patient 11 RSNs were detected in both condition A and B, including the ICE. Shown are the correlation matrices (Pearson's correlation) for the conditions A and B, the difference parameter ($\Delta\alpha$) matrix, which expresses the difference in functional connectivity between conditions A and B. Negative values of the difference parameter ($\Delta\alpha$) indicate that functional connectivity is larger in condition B compared to A. The matrix showing the absolute values of the differences in correlation between conditions A and B (i.e. the correlation difference matrix) for each combination of RSN components indicates that the functional connectivity in general is higher in condition B compared to A. Correlation values between the time series of the RSNs are in the range −0.4 to 0.4. The mean of the significant differences values ($\Delta\alpha$) in the matrix for the 45 min data are $\overline{\Delta\alpha} = -0.02 \pm 0.23$, while the mean of the absolute correlation difference values in the matrix is 0.20 ± 0.1.

The number of RSNs may be affected by differences in scan duration, compromising a comparison with earlier findings. Besides that, we are interested in epilepsy related changes in functional connectivity. Therefore we compared the analysis of the entire fMRI datasets of 45 min to that obtained with a selection of 10 min containing a maximum number of IEDs. Functional connectivity results for patient 4 for a 10 min fragment are shown in Fig. 4b. For the 10 min data selection only 7 RSNs were found, compared to 11 RSNs for the 45 min data. The mean of the significant differences values ($\Delta\alpha$) in the matrix for the 10 min data are $\bar{\Delta\alpha} = -0.11 \pm 0.32$, while the mean of the absolute correlation difference values in the matrix is 0.29 ± 0.20.

3.4. Group analysis

For comparison with the 10 min data an overview of the identified RSNs for the controls included in this study is shown in Fig. 5a. This figure illustrates that the number of RSNs varies considerable in between the subjects. There seems to be a relation of the number of detected RSNs with the age of the healthy control (the age is indicated at the vertical axis right). For the older subjects included in this study the number of RSN was less than for the younger ones, with on average 7.2 ± 2.9 RSNs identified. Note, however, that we did not find a similar effect for the patients included in this study (Fig. 5b and c). For the 10 min fragments of the patient data this is 6.7 ± 1.3 (the ICE is not included). The results presented in Fig. 5b and c indicate, furthermore, that there are no consistent differences between the RSNs present in condition A versus condition B. Their seems to be a slight overrepresentation in both conditions of the dDMN, hVN, PecN and pVN, similar as in the results of the healthy controls. For the entire datasets of 45 min on average 8.5 ± 1.9 RSNs were identified, which is significantly higher than for the 10 min fragments containing a maximum amount of IEDs ($p < 0.05$).

A group analysis on parameters derived from the functional connectivity matrices is performed to identify differences between conditions A and B on the group level. Therefore the mean difference parameter ($\overline{\Delta\alpha}$) has been calculated according to Eq. (3) and the results are shown in Fig. 6. The analysis of the entire 45 min datasets are shown in Fig. 6a

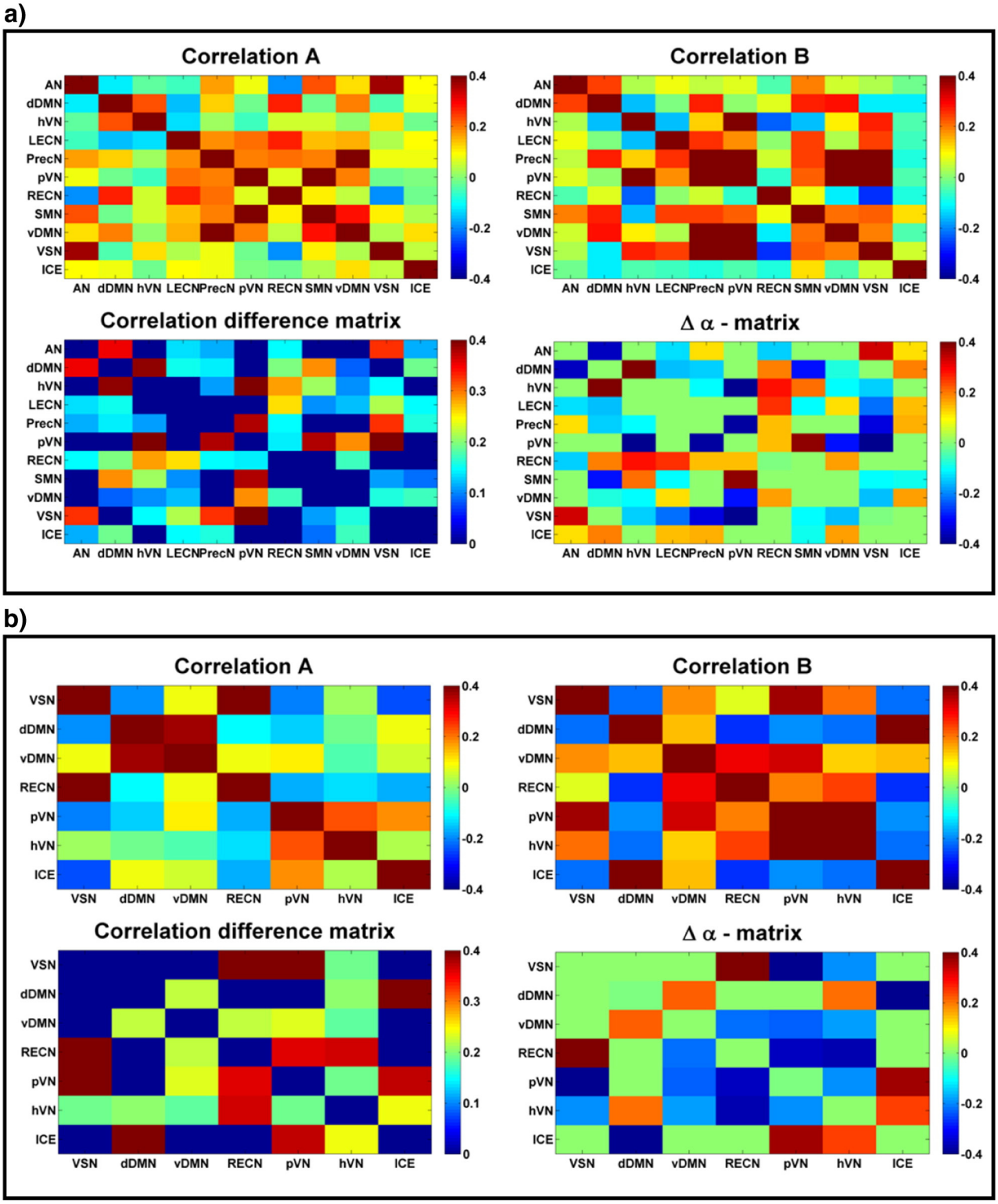

Fig. 4. Results for one patient (entire dataset (a) and 10 min data selection containing a maximum amount of IEDs (b)). Shown are the correlation matrices (Pearson's correlation) for conditions A and B, the functional connectivity difference ($\Delta\alpha$) matrix and the matrix with the absolute differences in correlation.

and the results of the 10 min data containing a maximum amount of IEDs in Fig. 6b. The values of the mean difference parameter for the 45 min data are $\overline{\Delta\alpha} = -0.05 \pm 0.06$, and for the 10 min data containing a maximum amount of IEDs this value is $\overline{\Delta\alpha} = -0.03 \pm 0.14$. A Wilcoxon signed rank test applied to the values indicates that the median of the $\overline{\Delta\alpha}$ values for the 45 min data are significantly different from zero at the 5% significance level. For the 10 min data this is not the case, probably because of the large variation in the mean difference parameter ($\overline{\Delta\alpha}$). Fig. 6a and b indicates that the mean difference parameter ($\overline{\Delta\alpha}$) values are negative for most patients in the data sets with IEDs, except for patient 3 in the case of the 45 and 10 min data, and for patients 2 and 7 for the 10 min dataset. A negative $\overline{\Delta\alpha}$ value means that the functional connectivity is on average higher in condition B compared to A.

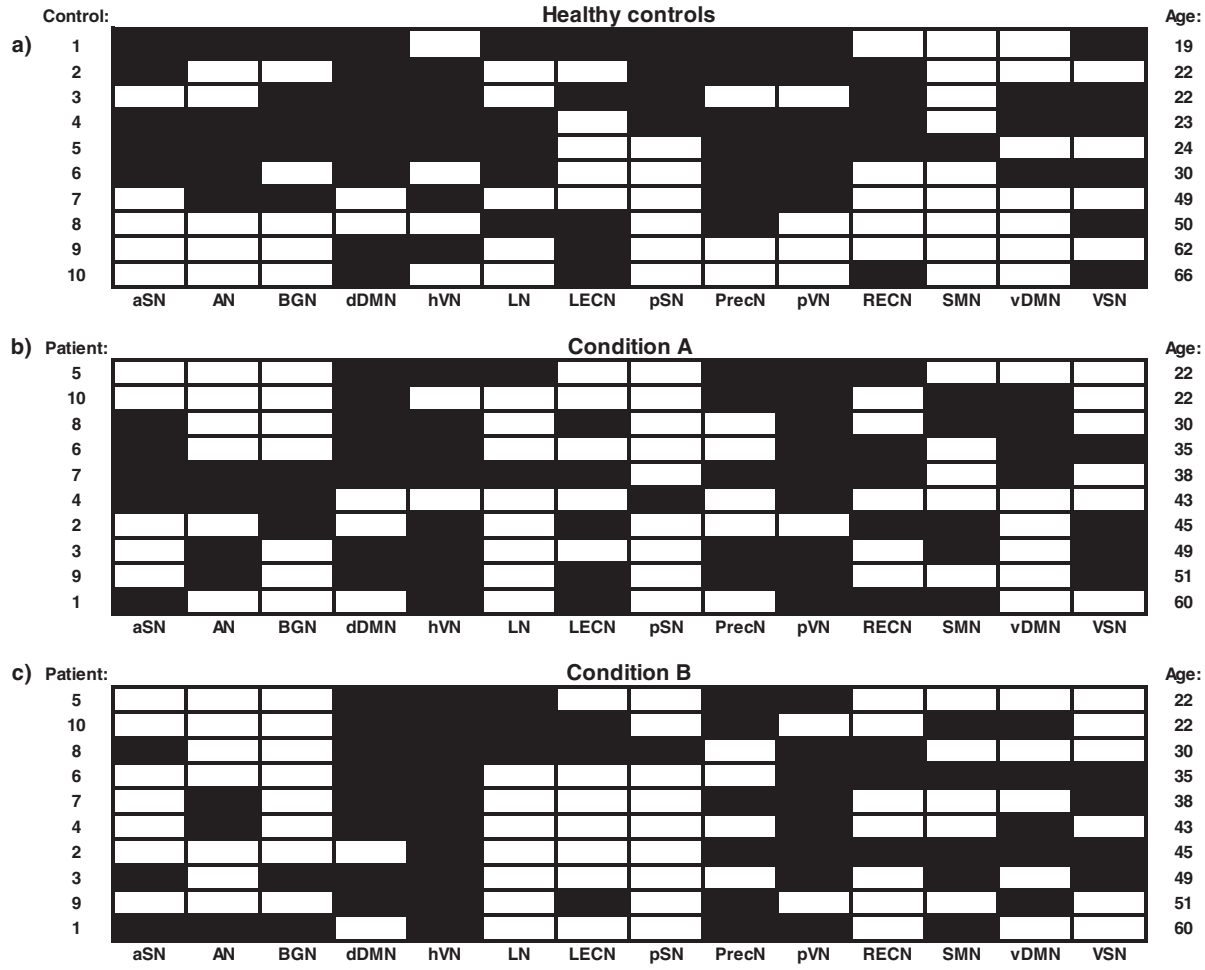

Fig. 5. Overview of detected RSNs for healthy controls, patients in condition A, and patients in condition B. RSN templates are: aSN = anterior salience network; AN = auditory network; BGN = basal ganglia network; dDMN = dorsal default mode network; hVN = higher visual network; LN = language network; LECN = left executive control network; pSN = posterior salience network, PrecN = precuneus network; pVN = primary visual network; RECN = right executive control network; SMN = sensorimotor network; vDMN = ventral default mode network; and VSN = visuospatial network. The black squares indicate which RSNs have been detected in the ten healthy volunteers, ten patients in condition A, and ten patients in condition B. The patient fMRI data have a 10 min length containing a maximum amount of IEDs. At the right the ages of the controls and patients are indicated.

In order to answer the question whether the results as presented in Fig. 6a are influenced by brain state, we summarized for all patients the periods of wakefulness (Wake), drowsiness (N1) and sleep (N_2, N_3) in Fig. 7. Group analysis indicated that there were no significant differences between wakefulness levels in conditions A and B ($p > 0.05$, Wilcoxon rank sum test). According to the observational parameters as mentioned earlier (continuous video observation, and a questionnaire) most patients were awake during scanning in both

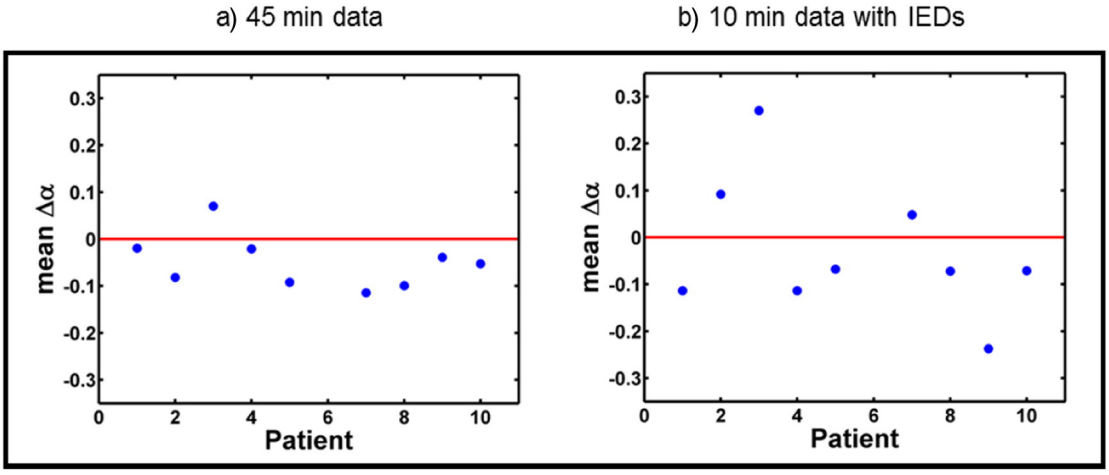

Fig. 6. Group analysis of functional connectivity results (entire dataset (a) and a 10 min selection containing a maximum amount of IEDs (b)). Mean difference parameter ($\Delta\alpha$) has been calculated for nine patients.

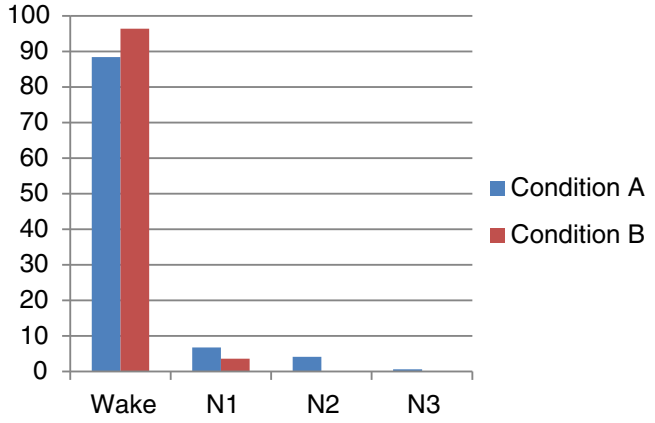

Fig. 7. Percentage of time spent in wakefulness (Wake), drowsiness (N1) and sleep (N2, N3) stages during the EEG–fMRI registrations for all ten patients, indicated for conditions A and B.

conditions A and B. Only patients 1, 5 and 7 had longer periods (>15 min) of drowsiness (N1), or (one patient) some periods of sleep (N2 and N3). Patient 1 was awake in condition A for 91% of the time and in condition B for 64% of the time (in N1 for the other periods). Patient 5 was awake in condition A for 39% and for 12%, 42% and 7% in N1, N2 and N3 stages, respectively. Patient 7 was awake in condition A for 55% of the time (the rest of the time in N1) and awake in condition B.

We also considered other physiological confounders that might influence the functional connectivity result. However, no systematic difference found in mean heart beat interval values between conditions A and B ($p > 0.05$) and therefore differences in functional connectivity are probably not caused by differences in heart rate. Also head movement influences functional connectivity (Van Dijk et al., 2012) but there was no systematic difference in head motion between both conditions ($p > 0.05$).

4. Discussion

In this study the effect of withdrawal of AEDs on the spatiotemporal characteristics of EEG related fMRI was explored. Our results show that the spatial extent of the epileptic network, as reflected by the ICE, is not affected by the withdrawal of AEDs. In previous studies it has been shown that the sensitivity of EEG–fMRI is dependent on the number of spikes (Salek-Haddadi et al., 2006; van Houdt et al., 2010). Although in our data the number of IEDs detected in the EEG is higher in condition B than in A, the increase is small and not significant. Nevertheless, the yield of EEG–fMRI was clearly higher in condition B and this might be explained by other factors than the number of identified IEDs. All patients, except one, showed an increase of functional connectivity in the condition after medication withdrawal. A possible explanation for the increase in functional connectivity after withdrawal of AEDs is given by the inhibiting effect of pharmacological drugs on signal transport in the brain (Rogawski, 2002). The AEDs reduce the synchronous firing of neuronal ensembles and therefore inhibit the propagation of seizures. This effect can be obtained by modulating sodium, calcium and potassium channels, elevation of the GABA concentration, or by potentiating GABA receptor currents. Because these mechanisms of action are influenced in the entire brain, and not only in the epileptic focus, the signal transport may be affected globally, which could be associated with an increased excitability of the brain. According to literature (e.g. Badawy et al., 2010) Transcranial Magnetic Stimulation (TMS) is the gold standard for measuring non-invasively the excitability of cortical neurons or intracortical circuits. This is achieved by exciting neuronal networks and assessing their immediate response, e.g., by measuring Motor Evoked Potentials (MEPs) or TMS-evoked EEG potentials (TEPs). To our knowledge TMS evoked responses have not yet been linked to the concept of rsFC studied with fMRI, which is a prerequisite for further interpretation of our findings. Excitability changes studied with combined TMS and EMG and rsFC based in fMRI on the same patient population could provide the support for a direct link between brain excitability and rsFC studied with fMRI.

The increase of functional connectivity after drug withdrawal did only reach the level of statistical significance when computations were based on the entire datasets of 45 min. When a 10 min subset of the data was used, this decrease was not significant, even when these data subsets were selected such that they contained the maximum number of IEDs. An additional analysis of 10 min data built from shorter fragments of fMRI data containing no IEDs did not show any significant trend in general functional connectivity either (data not shown). Apparently, the longer dataset is needed to be able to show the effect. We interpret these findings as a statistical effect where sensitivity to detect changes is increased by the longer scan durations. The fact that in the additional scans no visible IEDs were present in the co-registered EEG does not imply that epileptic activity does not play a role in the underlying mechanism. Following Hunyadi et al. (2013) and van Houdt et al. (2014), who found similar ICEs in data fragments containing no IEDs and fragments containing a maximum amount of IEDs, the fMRI signals of the additional scans might very well be affected by epileptic activity and therefore contribute to the observed increase in functional connectivity.

In this study functional connectivity has been calculated between resting state networks as identified by ICA in individual patients and controls. Damoiseaux et al. (2006) found that this resting state activity is consistent amongst different subjects, while Smith et al. (2009) showed that the functional networks found at 'rest' are comparable to those found during 'activation' in studies using fMRI and PET data. Shirer et al. (2012) demonstrated the classification of subject-driven cognitive processing using whole-brain functional connectivity between ROIs derived from 14 distinct RSNs obtained with ICA. The RSN templates of FIND laboratory (Shirer et al., 2012) were used in this study to detect independent component maps representing RSNs for individual patients and controls. The number of RSNs identified for 10 min data were comparable for patients and healthy controls in single patients. However, ICA of the 45 min datasets of the patients resulted in a larger number of identified RSN components, indicating that the identification of RSN components is affected by the length of the fMRI datasets.

Apart from the effect of IEDs on the functional connectivity, also other possible confounding effects should be taken into account. Firstly, not all patients used the same sort of AEDs (see Table 1). Our study was not designed to investigate differences in functional connectivity as a result of differences between sorts of drugs. Moreover, the investigation of the general effect of AEDs seems valid, because most AEDs reduce the synchronization in neuronal ensembles (Rogawski, 2002). Secondly, the patient group was heterogeneous with respect to age and gender. Biswal et al. (2010) showed that functional connectivity is dependent on age and gender, while Geerligs et al. (2014) found a decreased functional connectivity with increasing age. The result of our study indicates a decreased number of RSNs with age for the healthy control group. However, the same effect was not found for the patient group, which might be too small and too heterogeneous to draw further conclusions on these effects. Furthermore, in the condition were the patient was using the prescribed AEDs none of the patients had seizures, at least not in the 24 h before the EEG–fMRI measurement, while seizures occurred for a number of patients in the 24 h before the EEG–fMRI session after the withdrawal of AEDs (see Table 1). Therefore, a third confounding effect due to the increase of the number of seizures seems to be inevitable, since AED withdrawal increases, as is assumed in general, the number of seizures and results apparently in an increased rsFC.

Another confounding effect in resting state fMRI studies, as was shown in a recent paper of Tagliazucchi and Laufs (2014), is the difference in rsFC during wake versus sleep stages. We investigated, in

addition to the observational parameters the changes in brain state qualitatively. and found no systematic or significant differences in time spent in wakefulness, drowsiness and sleep stages during the 45 min of scanning between conditions A and B on the group level. However, in accordance to the observational parameters there are on the patient level differences in brain state for three of the patients studied. The percentage of time spent in drowsiness or sleep stages exceeded for two of these patients the percentage in wakefulness. However, according to Tagliazucchi and Laufs (2014) rsFC is in general higher in the stages N1 and N2, compared to wakefulness, thus suggesting that the increased rsFC of these patients in condition B related to A might be underestimated. Only in patient 1, who had periods of drowsiness (N1) in condition B and was awake in condition A, the increased rsFC possibly could be related to differences in brain state in conditions A and B. Finally, we investigated the general effect of drug withdrawal on rsFC based on a 45 min scanning session, which should be less sensitive to drifting in between brain states, like wakefulness, drowsiness and short periods of light sleep as found by Tagliazucchi and Laufs (2014) during resting state fMRI measurements. In order to be able to correct for brain stages based on quantitative EEG analysis we are working on methods (e.g. a double-layer electrode cap; Chowdhury et al., 2014) to remove the artifacts in the EEG due to scanning as much as possible, especially, the pulse artifacts, which are the most hard to remove.

Global effects of AEDs have also been studied using interictal EEG. Salinsky et al. (2003), for example, showed differences in the frequency content of the EEG signals. They found a shift of peak frequencies in the EEG spectra in conditions with medication compared to conditions without medication. Jacobs et al. (2012) investigated the number of high frequency oscillations occurring in conditions with and without medication and they found a significant increase in high frequency oscillations (HFOs) in the EEG after withdrawal of AEDs. These authors, however, indicated that the occurrence of spikes is not influenced by the usage of AEDs, but assumed that an increased number of seizures due to withdrawal are associated with an increase of IEDs, including HFOs. In general, the effect of AEDs on the number of IEDs is still under debate.

In conclusion, this study suggests that performing EEG–fMRI after withdrawal of AEDs may increase the EEG–fMRI yield. This yield increase is associated with an increase in functional connectivity between resting state networks, but not with an increased number of IEDs detected in the EEG. Contrary to the variable and inconsistent changes in the occurrence of IEDs in the EEG, as reported in literature, this study shows that the increase in rsFC after AED withdrawal is consistent over patients, suggesting the potential role for resting state fMRI in AED research.

Acknowledgments

This study is part of the Central Nervous System and Imaging (CSI) project that has received funding from the ENIAC Joint Undertaking (grant no. 120209), and the Devices for NeuroControl and NeuroRehabilitation (DeNeCor) project that has received funding from the ENIAC Joint Undertaking (grant no. 324257). The authors would like to thank Jan Verwoerd (clinical scientist at Philips Health care Best) for his contribution to the EEG–fMRI measurement procedures and Marlies Dolmans, Ine Keulen and Remco Berting for their contribution during the recording and annotation of the EEG–fMRI data. Furthermore, we would like to thank Roy Krijn and Peter Bijkerk for technical support and Stephan Meesters for his help on the fMRI data analysis.

Appendix 1

The purpose of the analysis is to detect whether changes in functional connectivity occurs, i.e. to test statistically whether the functional connectivity is different in condition A than in condition B. We could compute the correlation coefficients in conditions A and B, but there exists no test to assess whether this difference in correlations is statistically significant. Since a (normal) correlation coefficient is directly related to the statistical significance of the slope parameter of a least squares line fit procedure, we set up a general linear model for the concatenated time series and tested to what extend the concatenated time series could be explained by a single slope parameter or whether a different slope parameter for each part was statistically necessary, indicating that the slope and therefore the functional connectivity is changed between conditions A and B. Within the GLM theory, we therefore tested the statistical significance of the $\Delta\alpha$ parameter (see Fig. 8 for a graphical explanation of this parameter) by considering the partial correlation coefficient.

If the column vector $\mathbf{y}$ represents the fMRI time signal from one component after projecting out nuisance effects and $\mathbf{x}$ represents the

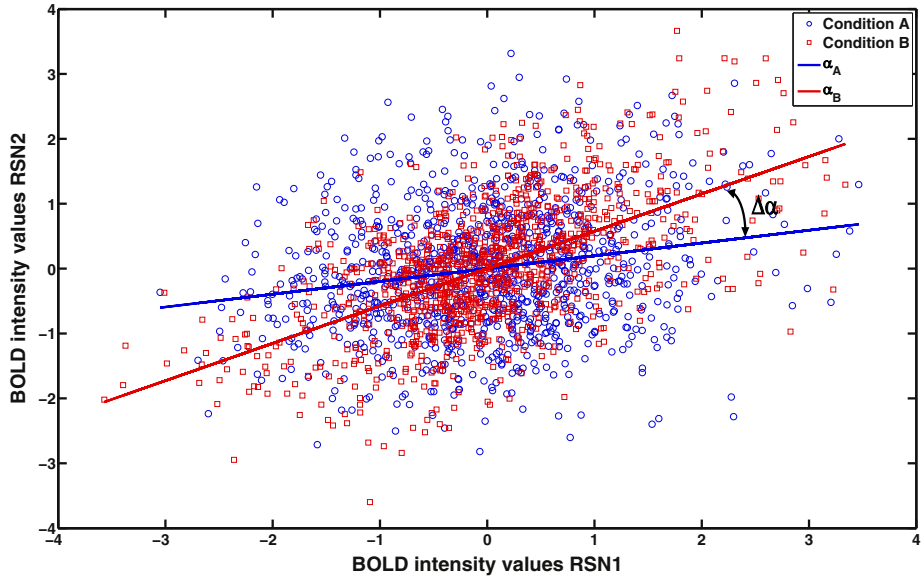

Fig. 8. Plot of BOLD response intensity values at times t_i (1075 time points (45 min fMRI)) of the mean BOLD time series from two RSNs, for conditions A (blue circles) and B (red squares) of one patient. The fitted slopes are indicated by blue (α_A) and red (α_B) lines. The difference in slopes represents the parameter $\Delta\alpha$.

corresponding quantity of another component, the simplest model by which these signals can be modeled is

$$\mathbf{y} = \phi\mathbf{e} + \alpha\mathbf{x} + \boldsymbol{\varepsilon} \tag{A1}$$

where $\mathbf{e}$ is a vector of ones, φ is a nuisance parameter and $\boldsymbol{\varepsilon}$ is the noise vector. In principle this model could be extended by adding non-linear and time shifted modifications of $\mathbf{x}$, but advantage of Eq. (A1) is that it leads to a symmetric connectivity matrix.

To detect statistical significant changes from condition A to B, the fMRI time series are concatenated and it is determined whether the combined data set needs a different slope parameter α (expressing the linear interdependence between two fMRI time series) by testing whether adding a parameter $\Delta\alpha$ improved the GLM estimate significantly, using a t-test. When the matrix P is a projector that sets all time points of data set B to 0, and leaves the time points of data set A unaffected, this idea can be described in a model as follows

$$\mathbf{y} = \phi_0\mathbf{e} + \phi_1 P\mathbf{e} + \alpha\mathbf{x} + \Delta\alpha P\mathbf{x} + \boldsymbol{\varepsilon}. \tag{A2}$$

The first two terms describe the offset and its jump, the third term describes the common slope of data sets A and B, whereas the fourth term is the parameter of interest, which describes the difference in the slope between conditions A and B, expressing the difference in linear interdependence between two fMRI time series between conditions A and B. Therefore, a significant change in connectivity exists when the following partial correlation coefficient ρ is significant

$$\rho = \frac{\mathbf{y}^T P_S P\mathbf{x}}{\sqrt{(\mathbf{y}^T P_S\mathbf{y})(\mathbf{x}^T P\mathbf{x})}}. \tag{A3}$$

Here $P_S = I - S(SS^T)^{inv}S^T$ and S is built from the three columns $S = (\mathbf{e},P\mathbf{e},\mathbf{x})$. In our analysis the IC time series are variance normalized and therefore the method is not sensitive to global scaling effects.

References

AASM, 2007. The AASM Manual for the Scoring of Sleep and Associated Events: Rules, Terminology and Technical Specifications. American Academy of Sleep Medicine, Westchester.

Aguirre, G.K., Zarahn, E., D'esposito, M.D., 1998. The variability of human, BOLD hemodynamic responses. Neuroimage 8 (4), 360–369. http://dx.doi.org/10.1006/nimg.1998.03699811554.

Badawy, R.A.B., Macdonell, R.A.L., Berkovic, S.F., Newton, M.R., Jackson, G.D., 2010. Predicting seizure control: cortical excitability and antiepileptic medication. Ann. Neurol. 67 (1), 64–73. http://dx.doi.org/10.1002/ana.2180620186859.

Bagshaw, A.P., Aghakhani, Y., Bénar, C.G., Kobayashi, E., Hawco, C., Dubeau, F., Pike, G.B., Gotman, J., 2004. EEG–fMRI of focal epileptic spikes: analysis with multiple haemodynamic functions and comparison with gadolinium-enhanced MR angiograms. Hum. Brain Mapp. 22 (3), 179–192. http://dx.doi.org/10.1002/hbm.2002415195285.

Beall, E.B., Lowe, M.J., 2010. The non-separability of physiologic noise in functional connectivity MRI with spatial ICA at 3T. J. Neurosci. Methods 191 (2), 263–276. http://dx.doi.org/10.1016/j.jneumeth.2010.06.02420600313.

Beckmann, C.F., Smith, S.M., 2004. Probabilistic independent component analysis for functional magnetic resonance imaging. I.E.E.E. Trans. Med. Imaging 23 (2), 137–152. http://dx.doi.org/10.1109/TMI.2003.82282114964560.

Biswal, B., Yetkin, F.Z., Haughton, V.M., Hyde, J.S., 1995. Functional connectivity in the motor cortex of resting human brain using echo-planar MRI. Magn. Reson. Med. 34 (4), 537–541. http://dx.doi.org/10.1002/mrm.19103404098524021.

Biswal, B.B., Mennes, M., Zuo, X.-N., Gohel, S., Kelly, C., Smith, S.M., Beckmann, C.F., Adelstein, J.S., Buckner, R.L., Colcombe, S., Dogonowski, A.-M., Ernst, M., Fair, D., Hampson, M., Hoptman, M.J., Hyde, J.S., Kiviniemi, V.J., Kötter, R., Li, S.-J., Lin, C.-P., Lowe, M.J., Mackay, C., Madden, D.J., Madsen, K.H., Margulies, D.S., Mayberg, H.S., McMahon, K., Monk, C.S., Mostofsky, S.H., Nagel, B.J., Pekar, J.J., Peltier, S.J., Petersen, S.E., Riedl, V., Rombouts, S.A.R.B., Rypma, B., Schlaggar, B.L., Schmidt, S., Seidler, R.D., Siegle, G.J., Sorg, C., Teng, G.-J., Veijola, J., Villringer, A., Walter, M., Wang, L., Weng, X.-C., Whitfield-Gabrieli, S., Williamson, P., Windischberger, C., Zang, Y.-F., Zhang, H.-Y., Castellanos, F.X., Milham, M.P., 2010. Toward discovery science of human brain function. Proc. Natl. Acad. Sci. U. S. A. 107 (10), 4734–4739. http://dx.doi.org/10.1073/pnas.091185510720176931.

Chowdhury, M.E.H., Mullinger, K.J., Glover, P., Bowtell, R., 2014. Reference layer artefact subtraction (RLAS): a novel method of minimizing EEG artefacts during simultaneous fMRI. Neuroimage 84, 307–319. http://dx.doi.org/10.1016/j.neuroimage.2013.08.03923994127.

Cole, D.M., Beckmann, C.F., Oei, N.Y.L., Both, S., van Gerven, J.M.A., Rombouts, S.A.R.B., 2013. Differential and distributed effects of dopamine neuromodulations on resting-state network connectivity. Neuroimage 78, 59–67. http://dx.doi.org/10.1016/j.neuroimage.2013.04.03423603346.

Cole, D.M., Smith, S.M., Beckmann, C.F., 2010. Advances and pitfalls in the analysis and interpretation of resting-state FMRI data. Front. Syst. Neurosci. 4, 8. http://dx.doi.org/10.3389/fnsys.2010.0000820407579.

Damoiseaux, J.S., Rombouts, S.A.R.B., Barkhof, F., Scheltens, P., Stam, C.J., Smith, S.M., Beckmann, C.F., 2006. Consistent resting-state networks across healthy subjects. Proc. Natl. Acad. Sci. U. S. A. 103 (37), 6. http://dx.doi.org/10.1073/pnas.060141710316945915.

de Munck, J.C., Gonçalves, S.I., Faes, T.J.C., Kuijer, J.P., Pouwels, P.J.W., Heethaar, R.M., Lopes da Silva, F.H., 2008. A study of the brain's resting state based on alpha band power, heart rate and fMRI. Neuroimage 42, 111–121.

de Munck, J.C., Gonçalves, S.I., Huijboom, L., Kuijer, J.P.A., Pouwels, P.J.W., Heethaar, R.M., Lopes da Silva, F.H., 2007. The hemodynamic response of the alpha rhythm: an EEG/fMRI study. Neuroimage 35 (3), 1142–1151. http://dx.doi.org/10.1016/j.neuroimage.2007.01.02217336548.

de Munck, J.C., van Houdt, P.J., Gonçalves, S.I., van Wegen, E., Ossenblok, P.P.W., 2013. Novel artefact removal algorithms for co-registered EEG/fMRI based on selective averaging and subtraction. Neuroimage 64, 407–415. http://dx.doi.org/10.1016/j.neuroimage.2012.09.02222995780.

Geerligs, L., Renken, R.J., Saliasi, E., Maurits, N.M., Lorist, M.M., 2014. A brain-wide study of age-related changes in functional connectivity. Cereb. Cortex 1–13 http://dx.doi.org/10.1093/cercor/bhu01224532319.

Genovese, C.R., Lazar, N.A., Nichols, T., 2002. Thresholding of statistical maps in functional neuroimaging using the false discovery rate. Neuroimage 15 (4), 870–878. http://dx.doi.org/10.1006/nimg.2001.103711906227.

Glover, G.H., Li, T.Q., Ress, D., 2000. Image-based method for retrospective correction of physiological motion effects in fMRI: RETROICOR. Magn. Reson. Med. 44 (1), 162–16710893535.

Huishi Zhang, C., Lu, Y., Brinkmann, B., Welker, K., Worrell, G., He, B., 2014. Lateralization and localization of epilepsy related hemodynamic foci using presurgical fMRI. Clin. Neurophysiol.

Hunyadi, B., Tousseyn, S., Mijović, B., Dupont, Van Huffel, P., Van Paesschen, S., De Vos, W., 2013. ICA extracts epileptic sources from fMRI in EEG-negative patients: A Retrospective Validation Study. PLOS ONE 8 (11), e78796. http://dx.doi.org/10.1371/journal.pone.007879624265717.

Bénar, C.-G, Grova, C., Kobayashi, E., Bagshaw, A.P., Aghakhani, Y., Dubeau, F., Gotman, J., 2006. EEG–fMRI of epileptic spikes: concordance with EEG source localization and intracranial EEG. Neuroimage 30 (4), 1161–1170. http://dx.doi.org/10.1016/j.neuroimage.2005.11.00816413798.

Jacobs, J., Staba, R., Asano, E., Otsubo, H., Wu, J.Y., Zijlmans, M., Mohamed, I., Kahane, P., Dubeau, F., Navarro, V., Gotman, J., 2012. High-frequency oscillations (HFOs) in clinical epilepsy. Prog. Neurobiol. 98 (3), 302–315. http://dx.doi.org/10.1016/j.pneurobio.2012.03.00122480752.

Khalili-Mahani, N., Zoethout, R.M.W., Beckmann, C.F., Baerends, E., de Kam, M.L., Soeter, R.P., Dahan, A., van Buchem, M.A., van Gerven, J.M.A., Rombouts, S.A.R.B., 2012. Effects of morphine and alcohol on functional brain connectivity during "resting state": a placebo-controlled crossover study in healthy young men. Hum. Brain Mapp. 33 (5), 1003–1018. http://dx.doi.org/10.1002/hbm.2126521391283.

LeVan, P., Gotman, J., 2009. Independent component analysis as a model-free approach for the detection of BOLD changes related to epileptic spikes: a simulation study. Hum. Brain Mapp. 30 (7), 2021–2031. http://dx.doi.org/10.1002/hbm.2064718726909.

Lund, T.E., Madsen, K.H., Sidaros, K., Luo, W.-L., Nichols, T.E., 2006. Non-white noise in fMRI: does modelling have an impact? Neuroimage 29 (1), 54–66. http://dx.doi.org/10.1016/j.neuroimage.2005.07.00516099175.

Masterton, R.A.J., Abbott, D.F., Fleming, S.W., Jackson, G.D., 2007. Measurement and reduction of motion and ballistocardiogram artefacts from simultaneous EEG and fMRI recordings. Neuroimage 37 (1), 202–211. http://dx.doi.org/10.1016/j.neuroimage.2007.02.06017582785.

Mueller, S., Costa, A., Keeser, D., Pogarell, O., Berman, A., Coates, U., Reiser, M.F., Riedel, M., Möller, H.J., Ettinger, U., Meindl, T., 2014. The effects of methylphenidate on whole brain intrinsic functional connectivity. Hum Brain Mapp 35 (11), 5379–5388. http://dx.doi.org/10.1002/hbm.2255724862742.

Rodionov, R., De Martino, F., Laufs, H., Carmichael, D.W., Formisano, E., Walker, M., Duncan, J.S., Lemieux, L., 2007. Independent component analysis of interictal fMRI in focal epilepsy: comparison with general linear model-based EEG-correlated fMRI. Neuroimage 38 (3), 488–500. http://dx.doi.org/10.1016/j.neuroimage.2007.08.00317889566.

Rogawski, M.A., 2002. Principles of Antiepileptic Drug Action. Antiepileptic Drugs. Lippincott Williams & Wilkins, Philadelphia, pp. 3–22.

Rosenkranz, K., Lemieux, L., 2010. Present and future of simultaneous EEG–fMRI. Magma 23 (5–6), 309–316. http://dx.doi.org/10.1007/s10334-009-0196-920101434.

Rummel, C., Verma, K., Schopf, R., Abela, V., Hauf, E., Zapata Berruecos, M., Wiest, J.F., 2013. Time course based artifact identification for independent components of resting-state fMRI. Front. Hum. Neurosci. 7, 1–8. http://dx.doi.org/10.3389/fnhum.2013.0021423734119.

Salek-Haddadi, A., Diehl, B., Hamandi, K., Merschhemke, M., Liston, A., Friston, K.J., Duncan, J.S., Fish, D.R., Lemieux, L., 2006. Hemodynamic correlates of epileptiform discharges: an EEG–fMRI study of 63 patients with focal epilepsy. Brain Res. 1088 (1), 148–166. http://dx.doi.org/10.1016/j.brainres.2006.02.09816678803.

Salek-Haddadi, A., Friston, K.J., Lemieux, L., Fish, D.R., 2003. Studying spontaneous EEG activity with fMRI. Brain Res. Brain Res. Rev. 43 (1), 110–133. http://dx.doi.org/10.1016/S0165-0173(03)00193-014499465.

Salinsky, M.C., Oken, B.S., Storzbach, D., Dodrill, C.B., 2003. Assessment of CNS effects of antiepileptic drugs by using quantitative EEG measures. Epilepsia 44 (8), 1042–1050. http://dx.doi.org/10.1046/j.1528-1157.2003.60602.x12887435.

Shirer, W.R., Ryali, S., Rykhlevskaia, E., Menon, V., Greicius, M.D., 2012. Decoding subject-driven cognitive states with whole-brain connectivity patterns. Cereb. Cortex 22 (1), 158–165. http://dx.doi.org/10.1093/cercor/bhr09921616982.

Smith, S.M., Fox, P.T., Miller, K.L., Glahn, D.C., Fox, P.M., Mackay, C.E., Filippini, N., Watkins, K.E., Toro, R., Laird, A.R., Beckmann, C.F., 2009. Correspondence of the brain's functional architecture during activation and rest. Proc. Natl. Acad. Sci. U. S. A. 106 (31), 13040–13045. http://dx.doi.org/10.1073/pnas.090526710619620724.

Tagliazucchi, E., Laufs, H., 2014. Decoding wakefulness levels from typical fMRI resting-state data reveals reliable drifts between wakefulness and sleep. Neuron 82 (3), 695–708. http://dx.doi.org/10.1016/j.neuron.2014.03.02024811386.

Tohka, J., Foerde, K., Aron, A.R., Tom, S.M., Toga, A.W., Poldrack, R.A., 2008. Automatic independent component labeling for artifact removal in fMRI. Neuroimage 39 (3), 1227–1245. http://dx.doi.org/10.1016/j.neuroimage.2007.10.01318042495.

Van 't Ent, D., Manshanden, I., Ossenblok, P., Velis, D.N., de Munck, J.C., Verbunt, J.P.A., Lopes da Silva, F.H., 2003. Spike cluster analysis in neocortical localization related epilepsy yields clinically significant equivalent source localization results in magnetoencephalogram (MEG). Clin. Neurophysiol. 114 (10), 1948–1962. http://dx.doi.org/10.1016/S1388-2457(03)00156-114499757.

Van Dijk, K.R., Sabuncu, M.R., Buckner, R.L., 2012. The influence of head motion on intrinsic functional connectivity MRI. NeuroImage 59 (1), 431–438. http://dx.doi.org/10.1016/j.neuroimage.2011.07.04421810475.

van Houdt, P.J., de Munck, J.C., Leijten, F.S.S., Huiskamp, G.J.M., Colon, A.J., Boon, P.A.J.M., Ossenblok, P.P.W., 2013. EEG–fMRI correlation patterns in the presurgical evaluation of focal epilepsy: a comparison with electrocorticographic data and surgical outcome measures. Neuroimage 75, 238–248. http://dx.doi.org/10.1016/j.neuroimage.2013.02.03323454472.

van Houdt, P.J., de Munck, J.C., Zijlmans, M., Huiskamp, G., Leijten, F.S.S., Boon, P.A.J.M., Ossenblok, P.P.W., 2010. Comparison of analytical strategies for EEG-correlated fMRI data in patients with epilepsy. Magn. Reson. Imaging 28 (8), 1078–1086. http://dx.doi.org/10.1016/j.mri.2010.03.02220471191.

van Houdt, P.J., Ossenblok, P.P.W., Colon, A.J., Boon, P.A.J.M., de Munck, J.C., 2012. A framework to integrate EEG-correlated fMRI and intracerebral recordings. Neuroimage 60 (4), 2042–2053. http://dx.doi.org/10.1016/j.neuroimage.2012.02.02322369995.

van Houdt, P.J., Ossenblok, P.P.W., Colon, A.J., Hermans, K.H.M., Verdaasdonk, R.M., Boon, P.A.J.M., de Munck, J.C., 2014. Are epilepsy-related fMRI components dependent on the presence of interictal epileptic discharges in scalp EEG? Brain Topogr. http://dx.doi.org/10.1007/s10548-014-0407-125315607.

ZijImans, M., Huiskamp, G., Hersevoort, M., Seppenwoolde, J.-H., van Huffelen, A.C., Leijten, F.S.S., 2007. EEG–fMRI in the preoperative work-up for epilepsy surgery. Brain 130 (9), 2343–2353. http://dx.doi.org/10.1093/brain/awm14117586868.